High-Power Fiber Lasers and Amplifiers Based on Multimode Interference

X. Zhu, A. Schülzgen, H. Li, L. Li, V. L. Temyanko, J. V. Moloney, and N. Peyghambarian, *Member, IEEE*

***Abstract*—In this paper, high-power fiber lasers and amplifiers based on multimode interference (MMI) in active large-core multimode optical fibers are proposed and their properties are investigated. Experimental results and simulations indicate that such fiber lasers and amplifiers are promising candidates for high-power miniature solid-state lasers. Utilization of the MMI leads to remarkable spectral and spatial features of fiber lasers and amplifiers such as generation of high-power diffraction-free beams.**

***Index Terms*—Multimode (MM) waveguides, optical fiber amplifiers, optical fiber devices, optical fiber filters, optical fiber interference, optical fiber lasers, optical fiber polarization.**

I. Introduction

POWER scaling of fiber lasers and amplifiers has attracted considerable interest in recent years because of the increasing demands for high-power or high-energy laser systems for various applications, including laser pumps, space communications, industrial welding and cutting, directed energy weapons, and high-energy physics researches. The two major approaches to obtain higher power or energy laser systems are either to boost the power level of a single-element fiber laser or amplifier, or to increase the element quantities in a beam combining system.

To effectively scale up the output power of a single-element fiber laser or amplifier, the power limits defined by the onset of nonlinear effects and optical damages have to be overcome. Increasing the area of the fundamental mode of the active fiber has always been the main approach. Single-mode (SM) active fibers with large mode area (LMA) have been realized either by precise control of the index step between the core and the cladding or by exploitation of the unique guiding properties of microstructured fibers. To date, for instance, 2-kW 1-μm silica-hosted [1], 10-W 2.78-μm ZBLAN-hosted [2], and 2-W 1.53-μm single-frequency phosphate-hosted [3] SM fiber lasers have been demonstrated using LMA SM fibers.

Alternatively, SM emission of a large-area fundamental mode from a multimode (MM) active fiber can be realized by introducing discrimination mechanisms that suppress the high-order transverse modes more than the fundamental mode. Fundamental-mode survival can be realized by special fiber designs [4]–[8] as well as laser cavity designs [9], [10].

Manuscript received August 30, 2008; revised October 26, 2008; accepted November 14, 2008. Current version published February 4, 2009. This work was supported by the National Sciences Foundation under Grant 0725479 and by the Arizona Technology and Research Initiative Fund.

The authors are with the College of Optical Sciences, University of Arizona, Tucson, AZ 85721 USA (e-mail: xszhu@email.arizona.edu; axel@optics.arizona.edu; hli@optics.arizona.edu; lli@optics.arizona.edu; vtemyanko@optics.arizona.edu; jml@acms.arizona.edu; nnp@u.arizona.edu).

Color versions of one or more of the figures in this paper are available online at http://ieeexplore.ieee.org.

Digital Object Identifier 10.1109/JSTQE.2008.2010270

Recently, a new concept to achieve single-transverse-mode output from a rare-earth-doped MM fiber has been proposed and demonstrated [11]. Utilizing the self-imaging effect of multimode interference (MMI) in the MM fiber section, SM output was obtained from a highly efficient diode-pumped MMI fiber laser consisting of a highly Er–Yb codoped phosphate MM fiber and a conventional SM fiber (SMF-28). In contrast to other approaches of obtaining SM emission from active MM fibers [4]–[10], this MMI fiber laser provided a perfect beam quality ($M^2 = 1.01$), an efficiency close to that of the MM fiber laser counterpart, and a narrow emission linewidth. However, the output of this first MMI fiber laser was limited to watt level by the active core diameter (25 μm) and the available pump power. Further power scaling may also be hampered by the low transition temperature ($\sim$600 °C) of the phosphate glass. In this paper, high-power MMI fiber lasers and amplifiers are proposed with active large-core ($>$50 μm) MM silica fibers.

The self-imaging effect of passive large-core ($>$50 μm) MM silica fiber has already been investigated and analyzed in detail [12]. Our calculations and experimental results have confirmed the feasibility of obtaining efficient single-transverse-mode emission from active large-core MM fibers. In this paper, critical features of MMI fiber lasers and amplifiers, such as slope efficiency, output spectrum, and beam quality, are studied. Moreover, unique characteristics of MMI fiber lasers and amplifiers including single-polarization, narrow-linewidth, and diffraction-free emission are demonstrated.

II. Principle of MMI Fiber Lasers and Amplifiers

When an arbitrary electromagnetic field is coupled into an MM waveguide, a specific set of eigenmodes of the MM waveguide is excited and each of them propagates along the waveguide independently with its own propagation. For the in-phase MMI, a reproduction of the input field (also called self-imaging) can be obtained at certain positions where the accumulated phase difference between any two excited modes is an integer multiple of 2π. Self-imaging in planar waveguides was first demonstrated by Ulrich and Ankele [13], and was found to be an inherent property of MM waveguides.

The self-imaging effect in MM waveguides implies that for an SM field incident on the input facet of an active MM waveguide, in-phase MMI results in an amplified SM field at the self-imaging plane in the MM waveguide. Applying self-imaging to obtain SM emission from an active MM planar waveguide has been proposed and demonstrated as a route to overcome the constraints of an active SM waveguide [14]–[19].

Although MMI in cylindrical optical fibers is more complicated than that in planar waveguides, perfect self-imaging of the

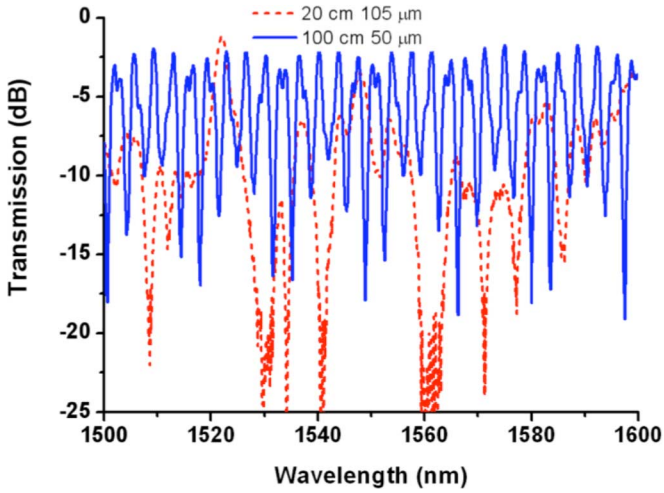

Fig. 1. Transmission spectra of two MMI structures consisting of a 100-cm-long 50-μm-core fiber (solid blue line) and a 20-cm-long 105-μm-core fiber (dashed red line) segment that is spliced in between two SMF-28 SM fiber segments.

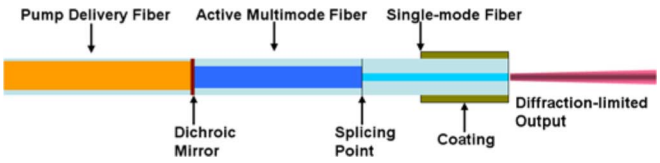

Fig. 2. Depiction of the proposed high-power MMI fiber laser in which the SM fiber is employed as the output fiber.

input SM field occurs when only a few modes are excited in the MM fiber segment [11], [12]. In analogy to MMI planar waveguide lasers, an efficient MMI fiber laser with diffraction-limited output has been demonstrated [11]. However, the core diameter of the active MM fiber was only 25 μm, which is close to core sizes of active SM fibers with low numerical aperture (NA). To boost the output of MMI fiber lasers, a larger core of the MM fiber is essential, in particular for silica fibers with relatively low rare earth doping levels.

When the corediameter of the MM fiber is larger than 50 μm, perfect self-imaging of the input field from a standard SM fiber (SMF-28) becomes practically impossible. However, a quasi-reproduction of the input field can still occur with a large self-imaging quality factor [12]. A typical transmission spectrum of an MMI structure consisting of a 100-cm-long MM silica fiber segment with a core diameter of 50 μm between two SMF-28 fibers is shown in Fig. 1 (the solid blue line). For certain wavelengths (with high transmission), self-imaging of the input SM field occurs and the propagation loss at the self-imaging wavelength is about 1.7 dB. When a 20-cm-long fiber segment with 105-μm core is used instead, the transmission spectrum shown in Fig. 1 (the dashed red line) changes considerably. Self-imaging is less frequent, but the propagation loss at the self-imaging wavelength of $\sim$1520 nm is only about 1.2 dB. Therefore, an MMI fiber laser cavity with low round-trip loss can still be constructed by splicing an SMF-28 fiber to a rare-earth-doped large-core MM fiber, as shown in Fig. 2. The MM pump delivery fiber is butt-coupled to the active MM fiber. A dielectric mirror that has high reflectivity at the lasing wavelength and high transmission at pump wavelength is deposited on the facet of the pump delivery fiber.

III. Features of MMI Fiber Lasers and Amplifiers

The self-imaging in passive large-core MM fibers has been investigated in detail in [12], and based on these previous results, high-power MMI fiber lasers and amplifiers utilizing active large-core MM fibers have been predicted. In this section, high-power MMI fiber lasers and amplifiers are demonstrated and their most important features are discussed.

A. Efficiency of MMI Fiber Lasers

When the MM fiber has a small core and a short length, the efficiency of an MMI fiber laser is very close to that of the corresponding MM fiber laser [11]. As the core diameter or the length of the MM fiber increases, the cavity loss will increase due to imperfect self-imaging and larger random mode conversion. To understand how these two factors affect the operation of an MMI fiber laser, the power distribution inside the fiber cavity, and the slope efficiency of an MMI fiber laser and its MM fiber laser counterpart can be investigated through simulations by combing a Rigrod analysis and a Digonnet model [20]. Although the cavity configuration and the oscillating modes inside the MM fiber segment are not identical for the MMI fiber laser and the MM fiber laser, we assume that this does not change the lasing dynamics, and our simulation based on effective absorption coefficients, cross sections, and excitation lifetimes is applicable to compare slope efficiencies between the MMI and MM fiber lasers.

In order to obtain high power from an MMI fiber laser, the parameters of a low-loss MM silica fiber codoped with Er and Yb ions are used in our calculations. According to the proposed setup of an MMI fiber laser shown in Fig. 2, the reflectivities of the cavity mirrors are $R_1 = 99\%$ and $R_2 = 4\%$ for the dielectric mirror and the cleaved SM fiber end facet, respectively. Using a Rigrod analysis and a Digonnet model, the governing equations for forward power $P^+(z)$ and backward power $P^-(z)$ in the cavity can be expressed as follows:

$$\frac{dP^+(z)}{dz} = \frac{\sigma_s \tau_f}{h\nu_p}\alpha_a P_p(z)\frac{F_p}{A_f}\frac{P_0 + P^+(z)}{1 + (P^+(z) + P^-(z))/P_s} - (\alpha_L + \alpha_{mc})P^+(z) \quad (1)$$

$$\frac{dP^-(z)}{dz} = -\frac{\sigma_s \tau_f}{h\nu_p}\alpha_a P_p(z)\frac{F_p}{A_f}\frac{P_0 + P^-(z)}{1 + (P^+(z) + P^-(z))/P_s} + (\alpha_L + \alpha_{mc})P^-(z). \quad (2)$$

In these equations, z represents the position in the fiber cavity. The pump power propagates according to $P_p(z) = P_p(0)\exp[-(\alpha_a + \alpha_p)z]$ after $P_p(0)$ is launched into the MM fiber section. Here, α_a is the effective absorption coefficient and α_p is the background loss of the fiber at the pump wavelength of 975 nm, α_L is the background loss at the laser wavelength of 1535 nm and α_{mc} is the loss due to the random mode conversion, A_f is the cross-sectional area of the fiber core, σ_s the

stimulated cross-section, $\tau_{\rm f}$ the excitation lifetime of the upper laser level, $h\nu_{\rm p}$ the pump photon energy, $h\nu_{\rm L}$ the laser photon energy, $F_{\rm p}$ the spatial overlap integral between pump and signal modes, $P_{\rm s} = (h\nu_{\rm L}/\sigma_{\rm s}\tau_{\rm f})A_{\rm f}$ the saturation output power, and $P_0 = Nh\nu_{\rm L}(\pi\Delta\nu_{\rm L}/2)$ the spontaneous emissions associated with N photons in the gain bandwidth $\Delta\nu_{\rm L}$.

The fourth Runge–Kutta method was used to do iterative calculations to solve the coupled differential equations for forward and backward powers in a cavity of length $L_{\rm f}$. By using the boundary conditions $P^+(0) = R_1P^-(0)$ and $P^+(L_{\rm f}) = R_2P^+(L_{\rm f})$, the boundary values in our simulations are given by, as shown (3), at the bottom of this page.

In addition, self-imaging quality at the splicing point $z_{\rm sp}$ is assumed leading to $P^+_{\rm SM}(z_{\rm sp}) = \eta P^+_{\rm MM}(z_{\rm sp})$ and $P^-_{\rm MM}(z_{\rm sp}) = P^-_{\rm SM}(z_{\rm sp})$. $P_{\rm SM}$ is the power inside the SM fiber, $P_{\rm MM}$ is the power inside the active MM fiber, and η is the power coupling efficiency from the MM fiber to the SM fiber.

The values of the parameters used in our simulations were set as $\alpha_{\rm p} = 6.5 \times 10^{-2}$ m^{-1}; $\alpha_{\rm L} = 3.2 \times 10^{-2}$ m^{-1}; $\sigma_{\rm s} = 5.7 \times 10^{-25}$ m^{-3}; $\tau_{\rm f} = 11$ ms; and $F_{\rm p} = 0.95$ for the MM fiber. The effective absorption coefficient $\alpha_{\rm a}$ has been calculated from the core absorption divided by the ratio between the area of the pump cladding and the area of the core. Although a core absorption of 1000 dB/m can be achieved in an Er–Yb codoped silica fiber and such a fiber laser has resulted in a slope efficiency of 41% [21], in our calculation, the core absorption coefficient is set to be 300 dB/m since it is large enough for an MMI fiber laser. This absorption can be adjusted and optimized by varying the Yb doping level in the active fiber core.

It is assumed that a commercial 105-μm-core fiber-coupled laser diode with an output power of 75 W is employed as the pump source. When a 50-μm MM fiber was used in the MMI structure, the loss due to mode conversion was measured to be 1.28 dB/m and η was -0.5 dB [12]. In Fig. 3, the forward power and the backward power inside the MMI fiber laser that consists of a 50-cm-long active MM fiber and a 10-cm-long SMF-28 fiber are plotted. For comparison, the forward power and the backward power inside the 50-cm-long MM fiber laser without the SMF-28 section are also plotted. Obviously, the powers inside the MM fiber segment of the MMI fiber laser are smaller than those of the MM fiber laser due to the loss of random mode conversion, and the output power of the MMI fiber laser is further reduced due to the imperfect self-imaging.

When a 105-μm MM fiber is used in the MMI structure, the loss due to mode conversion was measured to be 1.67 dB/m and η was -1 dB [12]. In Fig. 4, the forward power and the backward power inside the MMI fiber laser that consists of a 50-cm-long MM active fiber and a 10-cm-long SMF-28 fiber, and inside the corresponding 50-cm-long MM fiber laser are plotted. Due to mode conversion and imperfect self-imaging, the output power from the MMI fiber laser is only 65% of that of the corresponding MM fiber laser.

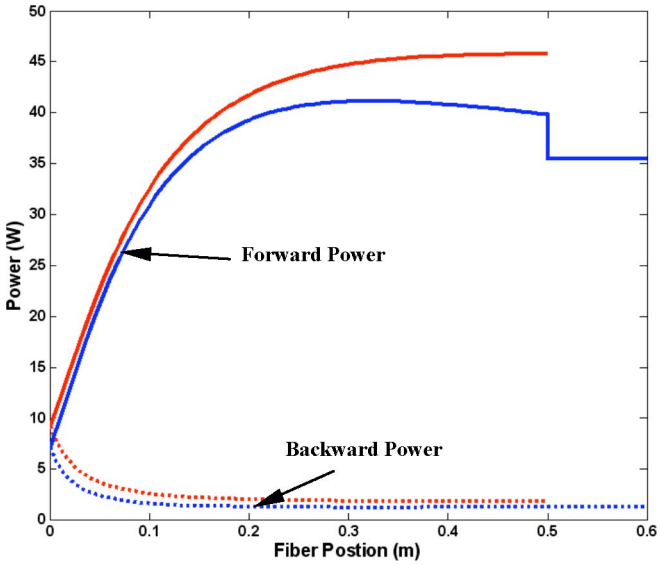

Fig. 3. Forward powers (solid lines) and backward powers (dotted lines) inside an MMI fiber laser that consists of a 50-cm-long 50-μm active MM fiber and a 10-cm-long SMF-28 fiber (blue), and inside its corresponding 50-cm-long MM fiber laser (red).

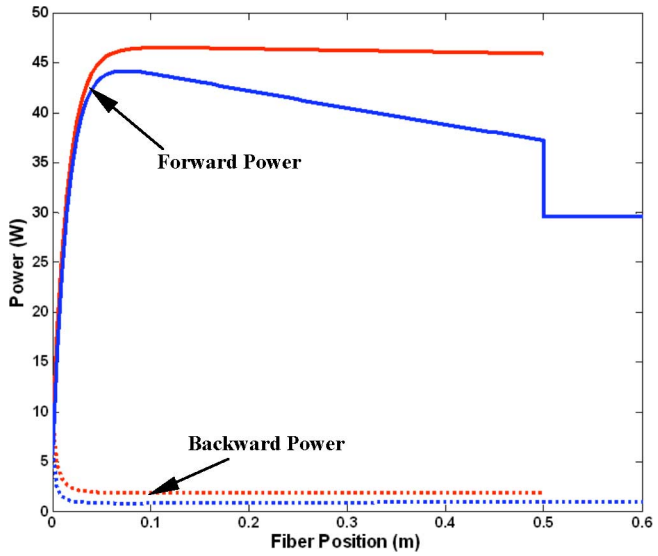

Fig. 4. Forward powers (solid lines) and backward powers (dotted lines) inside an MMI fiber laser that consists of a 50-cm-long 105-μm active MM fiber and a 10-cm-long SMF-28 fiber (blue), and inside its corresponding 50-cm-long MM fiber laser (red).

In Fig. 4, it is clear that the pump is almost absorbed within the first 10 cm of active fiber because of the effective core pumping scheme. Therefore, the length of the 105-μm active MM fiber segment can be as short as 10 cm. For this case, the forward powers and the backward powers inside the MMI fiber laser and the corresponding 10-cm-long MM fiber laser are plotted

$$P^+(L_{\rm f}) = \frac{-P_0(1+R_2) + \sqrt{P_0^2(1+R_2)^2 + 4R_2P^-(0)(P_0 + R_1P^-(0) + P_0R_1)}}{2R_2} \tag{3}$$

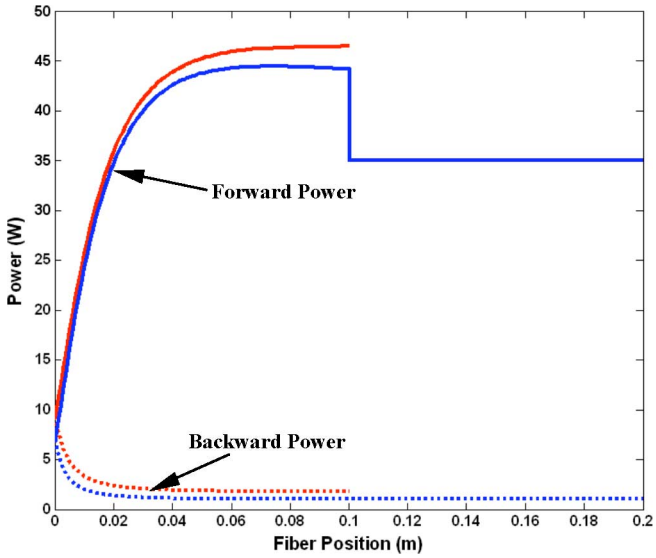

Fig. 5. Forward powers (solid lines) and backward powers (dotted lines) inside an MMI fiber laser that consists of a 10-cm-long 105-μm active MM fiber and a 10-cm-long SMF-28 fiber (blue), and inside its corresponding 10-cm-long MM fiber laser (red).

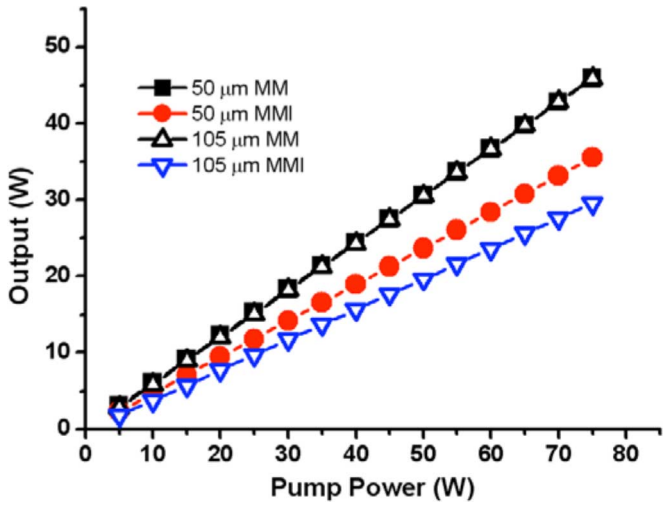

Fig. 6. Output power with respect to the pump power for an MMI fiber laser that consists of a 50-cm-long 50-μm (circles) or 105-μm active MM fiber (downward triangles) and a 10-cm-long SMF-28 fiber and their corresponding 50-cm-long MM fiber lasers (squares and upward triangles, respectively).

in Fig. 5. Note that the output power of the 105-μm MMI fiber laser reaches 75% of that of the corresponding MM fiber laser.

When the active MM fiber segment is 50 cm long, the output power with respect to the pump power for the MMI fiber lasers and their corresponding MM fiber lasers are plotted in Fig. 6. Because of the loss due to mode conversion and imperfect self-imaging, the slope efficiencies of the 50- and the 105-μm MMI fiber laser are 77% and 65% of those of their corresponding MM fiber lasers, respectively. In [12], we found that the mode conversion and the self-imaging quality can be improved via an SM fiber with a larger mode field diameter (MFD). When an SM fiber with an MFD of 23 μm (LMFD-10) was used, the loss due to the random mode conversion was only 0.5 dB/m [12].

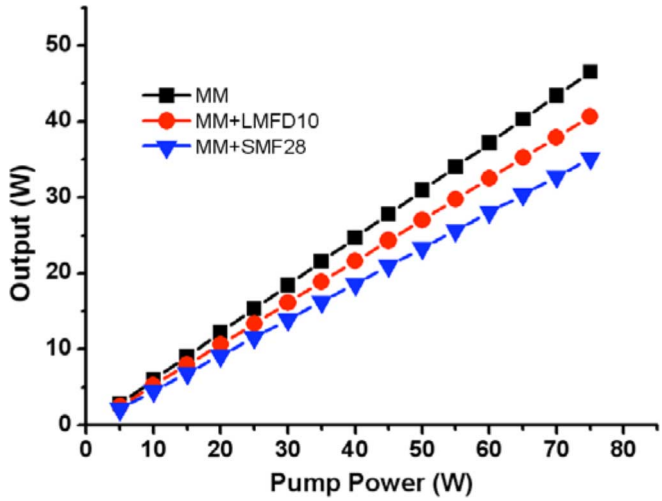

Fig. 7. Output power with respect to the pump power for an MMI fiber laser that consists of a 10-cm-long 105-μm active MM fiber and a 10-cm-long SMF-28 fiber (triangles) or a 10-cm-long LMFD-10 fiber (circles) and the corresponding 10-cm-long MM fiber laser (squares).

In Fig. 7, the output power with respect to the pump power for a 10-cm-long 105-μm MM fiber laser, an MMI fiber laser consisting of the 10-cm-long 105-μm MM fiber and a 10-cm-long SMF-28 fiber, and an MMI fiber laser consisting of a 10-cm-long 105-μm MM fiber and a 10-cm-long LMFD-10 fiber are plotted. When the SMF-28 fiber is used, the slope efficiency is 76% of the corresponding MM fiber laser. When the LMFD-10 fiber is used, the slope efficiency is increased to 87% of the corresponding MM fiber laser. We believe that the efficiency of the MMI fiber laser can be much closer to that of its corresponding MM fiber laser if the random mode conversion and the self-imaging quality are further improved. It is noted that, because of the filtering effect of the MMI as shown in Fig. 1, the amplified stimulated emission inside an MMI fiber should be restrained significantly.

B. Spectrum of MMI Fiber Lasers

Due to the filtering effect of MMI, the output spectrum of an MMI fiber laser always exhibits a unique feature—the MMI fiber laser oscillates only at wavelengths that satisfy the self-imaging condition. Therefore, the output spectrum of an MMI fiber can be tuned by changing the length of the MM fiber segment. In the first MMI fiber laser [11], a spectrum with one peak was observed as shown in Fig. 8. In comparison, a typical spectrum of an MM fiber laser is also plotted. Since there is no self-imaging around 1543 nm, there is no oscillation of the MMI laser at this wavelength. When an active MM fiber section with a length of 15 cm was used in the same MMI laser setup, a spectrum with two peaks was observed as shown in Fig. 9. Both experiments show that the output spectrum from an MMI fiber laser can be tailored through the length of the MM fiber section.

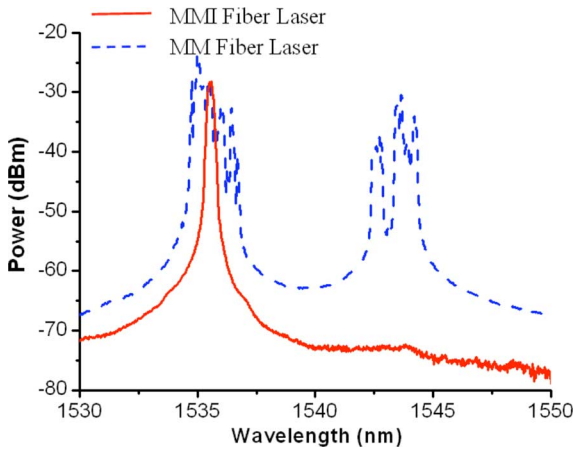

Fig. 8. Spectrum of an MMI fiber laser that utilizes a 10-cm-long 25-μm Er–Yb codoped phosphate fiber (solid red line) and that of the corresponding MM fiber laser (dashed blue line).

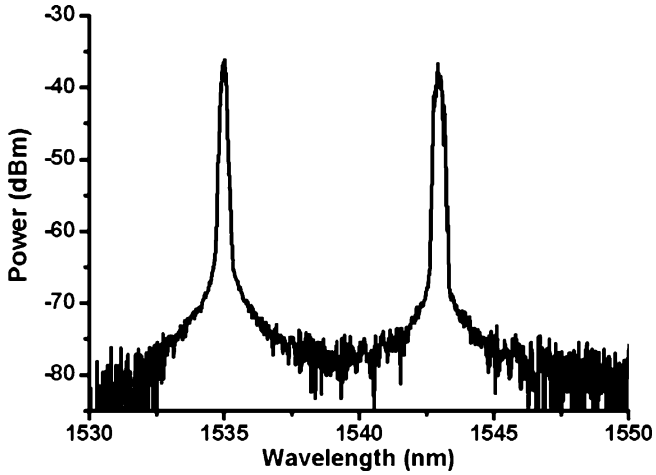

Fig. 9. Spectrum of an MMI fiber laser that utilizes a 15-cm-long 25-μm Er–Yb codoped phosphate fiber.

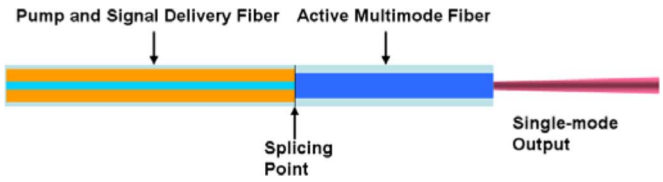

Fig. 10. Depiction of the proposed high-power MMI fiber amplifier in which the MM fiber is employed as the output fiber.

C. Beam Quality of MMI Fiber Lasers and Amplifiers

When a standard SM fiber is used as the output fiber as shown in Fig. 2, the output beam is strictly diffraction-limited and the beam quality (M^2) is equal to that of the SM fiber and can reach 1. In contrast to other methods of obtaining SM emission from MM active fiber, MMI fiber lasers not only offer a perfect beam quality, but also provide a flexible connectivity by using a standard SM fiber as the output delivery fiber.

On the other hand, an MMI fiber amplifier can also operate in a configuration shown in Fig. 10 in which the MM active fiber itself serves as the output fiber. In this case, the output power will be very close to that of the corresponding MM fiber laser. But the beam quality may be ruined due to imperfect self-imaging and random mode conversion. In order to investigate the beam quality of the output in this situation, a tunable semiconductor was employed as the input signal and a passive MM fiber was used to replace the active MM fiber. As shown in Fig. 11(a), the beam quality of the output at the self-imaging wavelength reached about 1.1 when a 50-μm MM fiber was used. When a 105-μm MM fiber was used, the beam quality of the output at the self-imaging wavelength was slightly worse, but still reaching about 1.3. It is noted that the M^2 measurement is truly meaningful only when the signal is at the self-imaging wavelength where near-Gaussian beams are generated. At other wavelengths, the output beam from the MM fiber exhibits a complicated profile with special propagation properties that will be discussed in Section V.

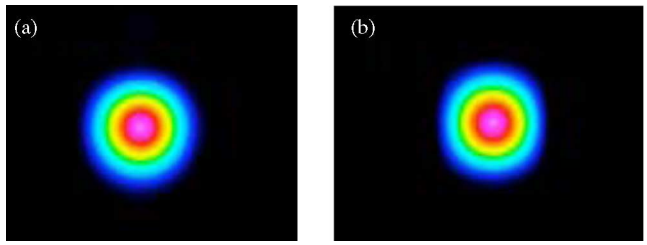

Fig. 11. Beam profiles of the proposed high-power MMI fiber amplifiers depicted in Fig. 10. (a) M^2 was about 1.1 when a 50-μm MM fiber was used. (b) M^2 was about 1.3 when a 105-μm MM fiber was used.

IV. Single-Polarization Output From an MMI Fiber Laser

In the next two sections, two applications based on the unique properties of MMI in optical fibers are proposed and demonstrated. The first is single-polarization emission with narrow linewidth and the second is the generation of high-power diffraction-free beams.

In general, to obtain single-polarization output from an all-fiber laser, a single-polarization SM fiber that guides only a single polarization state of the fundamental mode must be used. However, utilizing the spectral filtering effect of MMI, single-polarization SM emission can be obtained from an active MM fiber combined only with a polarization-maintaining fiber Bragg grating (PMFBG) without any other polarizing element.

A PMFBG is fabricated by writing the FBG onto a highly birefringent SM fiber. The transmission spectrum of a PMFBG, shown by a dotted green line in Fig. 12, always has two minima (two reflection peaks), which correspond to the two orthogonal linear polarization states. As a consequence, when the PMFBG is spliced with a conventional active SM fiber, a spectrum with two narrow-linewidth peaks is usually obtained and the output is randomly polarized. However, it is found that when the PMFBG was spliced to the output SMF-28 fiber in the MMI laser scheme of Fig. 2, a linearly polarized output with a 3-dB linewidth less than 0.1 nm was obtained. The linearly polarized output was verified by measuring the signal power through rotating a Glan–Taylor polarizer, and a polarization extinction ratio of about

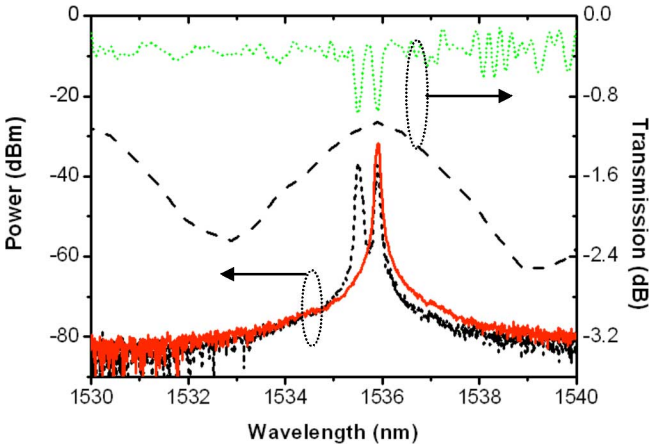

Fig. 12. Transmission spectra of a PMFBG (dotted green line) and an MMI structure consisting of a 20-cm-long 25-μm Er–Yb codoped MM phosphate fiber and two SMF-28 fibers (dashed line), and the output spectrum of an MMI fiber laser operating at single polarization state (solid red line) and random polarization state (short dashed line).

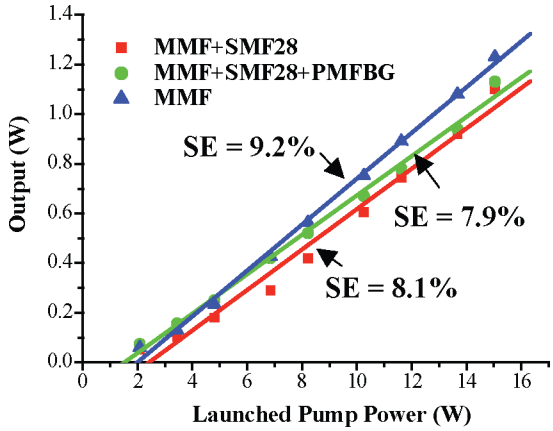

Fig. 13. Output power with respect to the launched pump power of an MMI fiber laser operating at single polarization state (green circles), its randomly polarized MMI fiber laser counterpart (red squares), and its MM fiber laser counterpart (blue triangles).

21 dB has been measured along the two orthogonal directions. The emission spectrum of the single-polarization-state operation is shown as a solid red line in Fig. 12. The emission peak is exactly correlated to one of the reflection peaks of the PMFBG.

The observed single-polarization-state operation is a direct consequence of the MMI filtering effect. The transmission spectrum of the MMI structure corresponding to the MMI fiber laser is shown by a dashed black line in Fig. 12. The overlap of the transmission peak of the MMI structure with the longer wavelength reflection peak of the PMFBG prevents the oscillation at the other shorter wavelength reflection peak and leads to single-polarization-state operation. Interestingly, when the pump delivery fiber is displaced a few tens of micrometers away from the in-contact butt-coupling position, an output spectrum with two peaks separated by about 0.4 nm was observed and is shown by a short dashed line in Fig. 12. Consequently, the output became randomly polarized. This phenomenon is caused by a shift of the MMI transmission peak into the center between the two reflection peaks of the PMFBG due to the longer MMI cavity [12]. In this situation, both polarization states were able to reach the lasing threshold and oscillate in the MMI laser cavity. Single-polarization-state operation at the shorter reflection peak of the PMFBG can also be obtained by moving the pump delivery fiber even further away. However, the output power becomes much lower because of the poor coupling of the pump light.

When the MM fiber length was accurately controlled, single polarization state was maintained even at the maximum pump level. The linearly polarized signal power as a function of pump power is shown in Fig. 13. The 7.9% slope efficiency of the MMI fiber laser in single-polarization operation (circles) is only slightly less than that of its randomly polarized MMI fiber laser counterpart (squares) and the MM fiber laser counterpart (triangles). The single-polarization-state operation of this MMI fiber laser may be more difficult to maintain as the pump power becomes much higher. However, when a larger core or a longer active MM fiber laser is used, single-polarization-state operation with much higher output is still possible since the filtering bandwidth of the corresponding MMI structure becomes narrower and the filtering isolation becomes much larger [12].

V. High-Power Diffraction-Free Emission

Diffraction-free beams, mainly represented by Bessel beams, can propagate in free space without significant beam spreading for a distance much longer than the normal Rayleigh range of a Gaussian beam [22], [23]. Bessel beams have attracted substantial interest because of their applications in optical guiding and manipulation, atomic optics, and nonlinear optics [23].

Excitingly, when we investigated the evolution of the intensity profile of the beam coming from a passive MMI device similar to the MMI fiber amplifier depicted in Fig. 10, diffraction-free propagation of the beam was observed. Here, we give a brief illustration of this effect and propose an active MMI device similar to that in Fig. 10 that can be utilized to generate high-power diffraction-free emission. A detailed analysis is in preparation and will be reported elsewhere [24].

Due to the mode orthogonality, only $LP_{0,n}$ modes are excited in the MM fiber segment when the input field is $LP_{0,1}$ mode (the fundamental mode of an SM fiber). The fields of the $LP_{0,n}$ modes in the fiber core are represented by apertured zero-order Bessel functions. Therefore, the MMI in the MM fiber can also be treated as the interference of Bessel fields and the output beam from the MM fiber is the superposition of Bessel-like beams. As analyzed and illustrated in [24], the higher the order n of the $LP_{0,n}$ modes, the closer the resemblance of a true Bessel beam. It is also found that the larger the core diameter of the MM fiber, the higher the $LP_{0,n}$ modes are excited [12], [24]. Therefore, when a large-core MM fiber is used in the MMI device shown in Fig. 10, the intensity evolution along the propagation direction exhibits an almost diffraction-free behavior.

For instance, when a single-frequency signal of 1570 nm from an SMF-28 fiber was launched to a 10-cm-long 50-μm MM fiber, the intensity profiles of the beam at selected distances from the MM fiber facet are shown in Fig. 14 (upper eight pictures). For

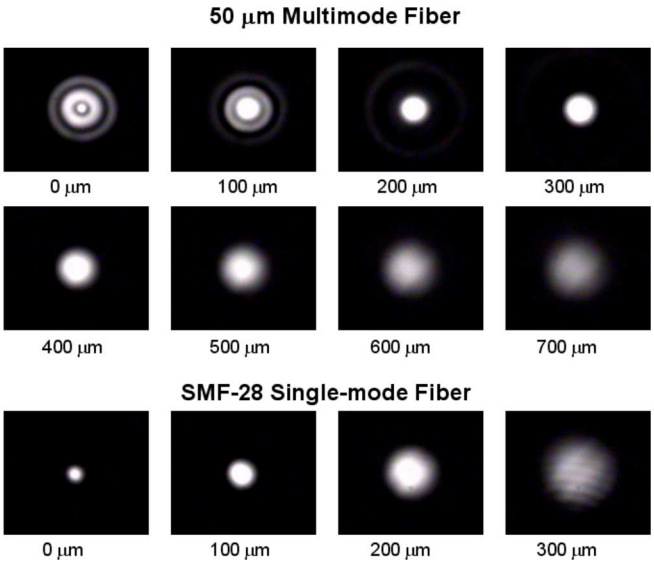

Fig. 14. Intensity profiles of the beam coming from a 50-μm MMI structure (upper pictures) and that from an SMF-28 fiber (lower pictures) at selected distances from the fiber facet.

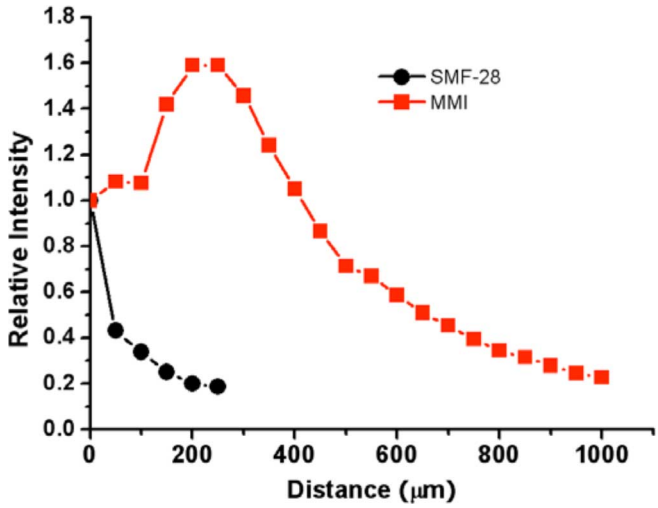

Fig. 15. Peak intensity of the central spot with respect to the distances from the fiber facet for the beam coming from a 50-μm MMI structure (square) and that from an SMF-28 fiber (circle).

comparison, the intensity profiles of the beam from the SMF-28 fiber are also shown in Fig. 14 (lower four pictures). Clearly, the propagation of the beam from the MMI fiber device exhibits a much smaller diffraction. The peak intensity of the central spot versus the propagation distance for the two cases is plotted in Fig. 15. For the beam coming from the SMF-28 fiber, the peak intensity reduces to a half value after propagating $\sim$100 μm as a consequence of diffraction. However, for the beam coming from the MMI fiber device, the peak intensity of the central spot can be maintained above half of its initial value for propagation distances of more than 600 μm.

Essentially, in comparison to other fiber devices proposed to generate diffraction-free beams [25], [26], our fiber device is not only simple and easy to fabricate, but also power-scalable. Normally, when a very small central spot size is desired, a small-core fiber has to be used [24]–[26]. That significantly decreases the power of the Bessel beam. However, by simply changing the MM fiber of the MMI structure from passive to active, as depicted in Fig. 10, high-power, nondiffracting beam can be obtained through stimulated amplification in the MM fiber. In other words, the MM fiber segment in the new device carries two functions simultaneously. One is to excite high-order $LP_{0,n}$ modes and the other is to amplify the excited modes. Based on our calculations and Limpert's experiments with rod-type fiber lasers [27], we believe that tens or even hundreds of watts of diffraction-free beams are feasible. That may considerably extend the applications of diffraction-free Bessel beams in nonlinear optics, high-energy physics, atomic optics, and microfabrication.

VI. Conclusion

MMI fiber lasers and amplifiers possess unique features that make them excellent candidates for compact and miniature solid-state lasers. Tens or even hundreds of watts of optical power can be generated from only a few tens of centimeters long MMI fiber lasers and amplifiers. Moreover, high-power diffraction-free emissions from MMI fiber lasers or amplifiers are possible and potentially have many new applications.

References

[1] V. Gapontsev, D. Gapontsev, N. Platonov, O. Shkurikhin, V. Fomin, A. Mashkin, M. Abramov, and S. Ferin, "2 kW CW ytterbium fiber laser with record diffraction-limited brightness," in *Proc. Conf. Lasers Electro-Opt. Eur.* Washington, DC: Opt. Soc. Amer., 2005, p. 508.

[2] X. Zhu and R. Jain, "10-W-level diode-pumped compact 2.78 μm ZBLAN fiber laser," *Opt. Lett.*, vol. 32, pp. 26–28, Jan. 2007.

[3] A. Schülzgen, L. Li, V. L. Temyanko, S. Suzuki, J. V. Moloney, and N. Peyhambarian, "Single-frequency fiber oscillator with watt-level output power using photonic crystal phosphate glass fiber," *Opt. Exp.*, vol. 14, pp. 7087–7092, Aug. 2006.

[4] H. L. Offerhaus, N. G. Broderick, D. J. Richardson, R. Sammut, J. Caplen, and L. Dong, "High-energy single-transverse-mode Q-switched fiber laser based on a multimode large-mode-area erbium-doped fiber," *Opt. Lett.*, vol. 23, pp. 1683–1685, Nov. 1998.

[5] J. M. Sousa and O. G. Okhotnikov, "Multimode Er-doped fiber for single-transverse-mode amplification," *Appl. Phys. Lett.*, vol. 74, pp. 1528–1530, Mar. 1999.

[6] U. Griebner, R. Koch, H. Schonnagel, and R. Grunwald, "Efficient laser operation with nearly diffraction-limited output from a diode-pumped heavily Nd-doped multimode fiber," *Opt. Lett.*, vol. 21, pp. 266–268, Feb. 1996.

[7] P. Wang, L. J. Cooper, J. K. Sahu, and W. A. Clarkson, "Efficient single-mode operation of a cladding-pumped ytterbium-doped helical-core fiber laser," *Opt. Lett.*, vol. 31, pp. 226–228, Jan. 2006.

[8] L. Dong, J. Li, and X. Peng, "Bend-resistant fundamental mode operation in ytterbium-doped leakage channel fibers with effective areas up to 3160 μm^2," *Opt. Exp.*, vol. 14, pp. 11512–11519, Nov. 2006.

[9] A. Polynkin, P. Polynkin, A. Schülzgen, M. Mansuripur, and N. Peyghambarian, "Watts-level, short all fiber laser at 1.5 μm with a large core and diffraction-limited output via intracavity spatial-mode filtering," *Opt. Lett.*, vol. 30, pp. 403–405, Feb. 2005.

[10] J. P. Koplow, D. A. V. Kliner, and L. Goldbergy, "Single-mode operation of a coiled multimode fiber amplifier," *Opt. Lett.*, vol. 25, pp. 442–444, Feb. 2000.

[11] X. Zhu, A. Schülzgen, H. Li, L. Li, Q. Wang, S. Suzuki, V. L. Temyanko, J. V. Moloney, and N. Peyghambarian, "Single-transverse-mode output from a fiber laser based on multimode interference," *Opt. Lett.*, vol. 33, pp. 908–910, May 2008.

[12] X. Zhu, A. Schülzgen, H. Li, L. Li, L. Han, J. V. Moloney, and N. Peyghambarian, "Detailed investigation of self-imaging in large-core

multimode optical fibers for application in fiber lasers and amplifiers," *Opt. Exp.*, vol. 16, pp. 16632–16645, Oct. 2008.
[13] R. Ulrich and G. Ankele, "Self-imaging in homogeneous planar optical waveguides," *Appl. Phys. Lett.*, vol. 27, pp. 337–339, Sep. 1975.
[14] K. Hamamoto, E. Gini, C. Holtmann, and H. Melchior, "Single-transverse-mode active multi-mode-interferometer 1.45 μm high power laser diode," *Appl. Phys. B*, vol. 73, pp. 571–574, 2001.
[15] H. J. Baker, J. R. Lee, and D. R. Hall, "Self-imaging and high-beam-quality operation in multi-mode planar waveguide optical amplifiers," *Opt. Exp.*, vol. 10, pp. 297–302, Mar. 2002.
[16] W. S. Pelouch, D. D. Smith, J. E. Koroshetz, I. T. Mckinnie, J. R. Unternahrer, S. W. Henderson, and W. R. Scharpf, "Self-imaging in waveguide lasers and amplifiers," in *Proc. OSA Top. Meeting Adv. Solid State Lasers*. Washington, DC: Opt. Soc. Amer., 2002, pp. 6–9.
[17] I. T. Mckinnie, J. E. Koroshetz, W. S. Pelouch, D. D. Smith, J. R. Unternahrer, S. W. Henderson, and M. Wright, "Self-imaging waveguide Nd:YAG laser with 58% slope efficiency," in *Proc. OSA Top. Meeting Adv. Solid State Lasers*. Washington, DC: Opt. Soc. Amer., 2002, pp. 262–263.
[18] I. T. Mckinnie, B. E. Callicoatt, C. Wood, J. E. Koroshetz, J. R. Unternahrer, M. L. Tartaglia, S. E. Christensen, O. J. Koski, M. Hinckley, M. J. Bellanca, E. Schneider, and D. D. Smith, "Self-imaging waveguide lasers," in *Proc. Conf. Lasers Electro-Opt.*, 2005, pp. 319–321, Paper CMS1.
[19] V. Raghunathan, H. Renner, R. R. Rice, and B. Jalali, "Self-imaging silicon Raman amplifier," *Opt. Exp.*, vol. 15, pp. 3396–3408, Mar. 2007.
[20] X. Zhu and R. Jain, "Numerical analysis and experimental result of high-power Er/Pr:ZBLAN 2.7 μm fiber lasers with different pumping designs," *Appl. Opt.*, vol. 45, pp. 7118–7125, Sep. 2006.
[21] D. Y. Shen, J. K. Sahu, and W. A. Clarkson, "Highly efficient Er, Yb-doped fiber laser with 188 W free-running and $>$100 W tunable output power," *Opt. Exp.*, vol. 13, pp. 4916–4921, Jun. 2005.
[22] J. Durnin, "Exact solutions for nondiffracting beams. I. The scalar theory," *J. Opt. Soc. Amer. A*, vol. 4, pp. 651–654, Apr. 2004.
[23] D. Mcgloin and K. Dholakia, "Bessel beams: Diffraction in a new light," *Contemp. Phys.*, vol. 46, pp. 15–28, Jan. 2005.
[24] X. Zhu, A. Schülzgen, L. Li, and N. Peyghambarian, "Generation of controllable nondiffracting beams using multimode optical fibers," *Opt. Lett.*, submitted for publication.
[25] T. Grosjean, S. S. Saleh, M. A. Suarez, I. A. Ibrahim, V. Piquerey, D. Charraut, and P. Sandoz, "Fiber microaxicons fabricated by a polishing technique for the generation of Bessel-like beams," *Appl. Opt.*, vol. 46, pp. 8061–8067, Nov. 2007.
[26] S. Ramachandran and S. Ghalmi, "Diffraction-free, self-healing Bessel beams from fibers," presented at the Conf. Lasers Electro-Opt./Quantum Electron. Laser Sci. Conf., San Jose, CA, 2008, Paper CPDB5.
[27] J. Limpert, N. D. Robin, I. M. Honninger, F. Salin, F. Roser, A. Liem, T. Schreiber, S. Nolte, H. Zellmer, A. Tunnermann, J. Broeng, A. Petersson, and C. Jakobsen, "High-power rod-type photonic crystal fiber laser," *Opt. Exp.*, vol. 13, pp. 1055–1058, Feb. 2005.

X. Zhu received the B.S. degree in physics and the M.S. degree in optical information processing from Nankai University, Tianjin, China, in 1996 and 1999, respectively, and the second M.S. degree in fiber devices from the University of New Mexico, Albuquerque, in 2004. He is currently working toward the Ph.D. degree in the area of fiber lasers and amplifiers at the University of Arizona, Tucson.

During 1999–2001, he was an Optical Engineer at Wuhan Research Institute of Telecommunications and Posts, Wuhan, China, where he was engaged in research of erbium-doped fiber amplifiers (EDFAs) and passive fiber devices for optical communications. He was also with the University of New Mexico, where his work focused on an all-fiber polarization transformer, mid-infrared fiber lasers and amplifiers, and stimulated Brillouin scattering in optical fibers. His current research interests include polarization states of laser arrays, fiber lasers and amplifiers based on multimode interference, narrow-linewidth mid-infrared fiber lasers, and nanostructured fibers.

A. Schülzgen received the Ph.D. degree in experimental physics from Humboldt-University Berlin, Berlin, Germany, in 1992.

During 1992–1995, he was a Research Fellow at Trinity College, Dublin, Ireland, and Humboldt-University Berlin, where he studied optical properties of low-dimensional semiconductor quantum structures. In 1996, he joined the University of Arizona, Tucson, where he is currently a Research Professor at the College of Optical Sciences. His current research interests include the investigation of advanced micro- and nanostructured materials, novel nonlinear optical effects, ultrafast optics, and laser development.

H. Li, photograph and biography not available at the time of publication.

L. Li, photograph and biography not available at the time of publication.

V. L. Temyanko, photograph and biography not available at the time of publication.

J. V. Moloney received the Ph. D degree from the University of Western Ontario, London, ON, Canada, in 1977.

He is currently with the College of Optical Sciences, University of Arizona, Tucson. His current research interests include mathematical modeling and simulation of photonics systems including semiconductor lasers, fiber lasers, photonic Bragg and photonic crystal fibers; fundamental theory of semiconductor lasers including microscopic physics; modeling high-power femtosecond atmospheric light strings; nonlinear theory of partial differential equations and chaos synchronization in extended complex spatiotemporal interacting systems; and sophisticated algorithm development for large-scale computational photonics systems simulations including adaptive mesh refinement and parallelization on distributed and shared memory supercomputer platforms.

N. Peyghambarian (M'04) received the Ph.D. degree from Indiana University, Bloomington, in 1982.

He is currently with the College of Optical Sciences, University of Arizona, Tucson. His current research interests include optical telecommunication, fiber optics, fiber amplifiers and fiber lasers, integrated optics including waveguide amplifiers, lasers, modulators; femtosecond laser spectroscopy and dynamics of optical phenomena in semiconductors and organic materials; nonlinear photonics and high-speed optical switching; characterization of optical materials in terms of speed and nonlinearities; and polymer optoelectronics, photorefractive polymers, and organic light-emitting diodes and lasers.

Dr. Peyghambarian is a Fellow of the American Physical Society, the Optical Society of America (OSA), and the International Society for Optical Engineers (SPIE).